

## Small Fermi Pockets Intertwined with Charge Stripes and Pair Density Wave Order in a Kagome Superconductor


Hong Li,<sup>1,\*</sup> Dongjin Oh,<sup>2,\*</sup> Mingu Kang,<sup>2,\*</sup> He Zhao,<sup>1</sup> Brenden R. Ortiz,<sup>3</sup> Yuzki Oey,<sup>3</sup> Shiang Fang,<sup>2</sup> Zheng Ren,<sup>1</sup> Chris Jozwiak,<sup>4</sup> Aaron Bostwick,<sup>4</sup> Eli Rotenberg,<sup>4</sup> Joseph G. Checkelsky,<sup>2</sup> Ziqiang Wang,<sup>1</sup> Stephen D. Wilson,<sup>3</sup> Riccardo Comin,<sup>2,†</sup> and Ilija Zeljkovic<sup>1,‡</sup>

<sup>1</sup>Department of Physics, Boston College, Chestnut Hill, Massachusetts 02467, USA

<sup>2</sup>Department of Physics, Massachusetts Institute of Technology, Cambridge, Massachusetts 02139, USA

<sup>3</sup>Materials Department, University of California Santa Barbara, Santa Barbara, California 93106, USA

<sup>4</sup>Advanced Light Source, E. O. Lawrence Berkeley National Laboratory, Berkeley, California 94720, USA

 (Received 27 March 2023; revised 13 June 2023; accepted 24 July 2023; published 15 September 2023)

The kagome superconductor family  $AV_3Sb_5$  ( $A = \text{Cs, K, Rb}$ ) emerged as an exciting platform to study exotic Fermi surface instabilities. Here, we use spectroscopic-imaging scanning tunneling microscopy (SI-STM) and angle-resolved photoemission spectroscopy (ARPES) to reveal how the surprising cascade of higher- and lower-dimensional density waves in  $\text{CsV}_3\text{Sb}_5$  is intimately tied to a set of small reconstructed Fermi pockets. ARPES measurements visualize the formation of these pockets generated by a 3D charge density wave transition. The pockets are connected by dispersive  $q^*$  wave vectors observed in Fourier transforms of STM differential conductance maps. As the additional 1D charge order emerges at a lower temperature,  $q^*$  wave vectors become substantially renormalized, signaling further reconstruction of the Fermi pockets. Remarkably, in the superconducting state, the superconducting gap modulations give rise to an in-plane Cooper pair density wave at the same  $q^*$  wave vectors. Our work demonstrates the intrinsic origin of the charge stripes and the pair density wave in  $\text{CsV}_3\text{Sb}_5$  and their relationship to the Fermi pockets. These experiments uncover a unique scenario of how Fermi pockets generated by a parent charge density wave state can provide a favorable platform for the emergence of additional density waves.

DOI: [10.1103/PhysRevX.13.031030](https://doi.org/10.1103/PhysRevX.13.031030)

Subject Areas: Condensed Matter Physics,  
Strongly Correlated Materials,  
Superconductivity

### I. INTRODUCTION

Correlated electron systems are often characterized by coexisting electronic orders vying for the same electronic states at the Fermi level. As a result, the residual Fermi surface exhibits smaller Fermi surfaces, or “pockets,” that govern many aspects of the low-energy physics. Identifying the existence of such pockets and understanding their renormalization driven by the emergent orders has been of immense interest in many complex solid-state systems. In cuprate superconductors, for example, there has been a longstanding debate about whether Fermi pockets existed, in an attempt to understand their connection to the

correlated liquid states emerging upon doping the parent Mott insulating phase [1–4].

Kagome superconductors in the  $AV_3Sb_5$  [5–8] family recently emerged as a new materials platform to theoretically [9–17] and experimentally [18–32] study exotic correlated and topological quantum states intertwined with Fermi surface instabilities. The rich array of electronic phenomena observed includes an unusual number of density waves with varying morphology and dimensionality, which onset at different temperatures upon cooling down and all coexist with superconductivity at low temperature. This includes the 3D charge density wave (CDW) with a  $2a_0$ -by- $2a_0$  period in the kagome plane (onset temperature  $T^* \sim 70$ – $100$  K [6,8,27,32–34]), a  $4a_0$  charge-stripe order ( $T_{4a_0} \sim 50$ – $60$  K [19]), and a  $4a_0/3$ -by- $4a_0/3$  Cooper pair density wave ( $T_c \sim 3$ – $4$  K [25]). The formation of the 3D CDW at  $T^*$  has been well established and explored by a variety of bulk probes [27,32,35,36], and its  $2a_0$  in-plane wavelength is expected to naturally arise on a hexagonal lattice [37]. In contrast, the surprising emergence of lower-dimensional density waves—the 1D  $4a_0$  charge stripes [19] and the in-plane pair density wave [25]—has been difficult to capture by the same bulk-sensitive tools.

\*These authors contributed equally to this work.

†Corresponding author: [rcomin@mit.edu](mailto:rcomin@mit.edu)

‡Corresponding author: [ilija.zeljkovic@bc.edu](mailto:ilija.zeljkovic@bc.edu)

Published by the American Physical Society under the terms of the [Creative Commons Attribution 4.0 International license](https://creativecommons.org/licenses/by/4.0/). Further distribution of this work must maintain attribution to the author(s) and the published article’s title, journal citation, and DOI.

This prompted an intense debate in the community on whether these states are intrinsic to the kagome lattice or have a different origin, e.g., a surface reconstruction [38,39]. Recent theory [15] has predicted that small Fermi pockets generated by the high-temperature CDW transition could be instrumental in the subsequent creation of exotic density waves at lower temperatures. In principle, this would lead to distinct fingerprints in the bulk electronic structure of the kagome bands associated with the transitions, but this is yet to be uncovered.

Here, we use a combination of angle-resolved photoemission spectroscopy (ARPES) and spectroscopic-imaging scanning tunneling microscopy (SI-STM) to unveil an intimate connection between density waves and reconstructed Fermi pockets in  $AV_3Sb_5$ . Our ARPES measurements reveal six small ellipsoidal holelike pockets generated by the  $2 \times 2$  CDW state forming at  $T^*$ . Scattering between these pockets leads to new, dispersive wave vectors  $\mathbf{q}^*$  in SI-STM measurements, oriented along each reciprocal lattice direction. While the three  $\mathbf{q}^*$  peaks all lie along the  $\Gamma$ -M directions of the original Brillouin zone when the  $4a_0$  charge-stripe order is absent, we discover that the morphology of these scattering peaks

changes dramatically when the charge-stripe order sets in. Namely, the dispersive nature of one  $\mathbf{q}^*$  peak becomes markedly suppressed, while the other two  $\mathbf{q}^*$  peaks remain dispersive and exhibit a slight deviation from the high-symmetry axes. This strongly suggests further reconstruction of the pockets as the charge-stripe order emerges, which could explain some of the smaller frequencies in quantum oscillation experiments of  $CsV_3Sb_5$  [35,36,40–43]. Remarkably, the Cooper pair density wave [25] that condenses in the superconducting state emerges at the same  $\mathbf{q}^*$  wave vectors that connect the hole pockets in reciprocal space. Our experiments reveal a direct link between vanadium kagome orbital-derived Fermi pockets, an inherent feature of the bulk electronic band structure, and the surprising cascade of lower-dimensional density waves in  $AV_3Sb_5$ .

## II. RESULTS

Bulk single crystals of  $AV_3Sb_5$  exhibit a layered structure consisting of  $V_3Sb_5$  layers stacked between A-site alkali metal layers [Fig. 1(a)]. The crystals tend to cleave between the A-site layer and the Sb layer (Sec. IV),

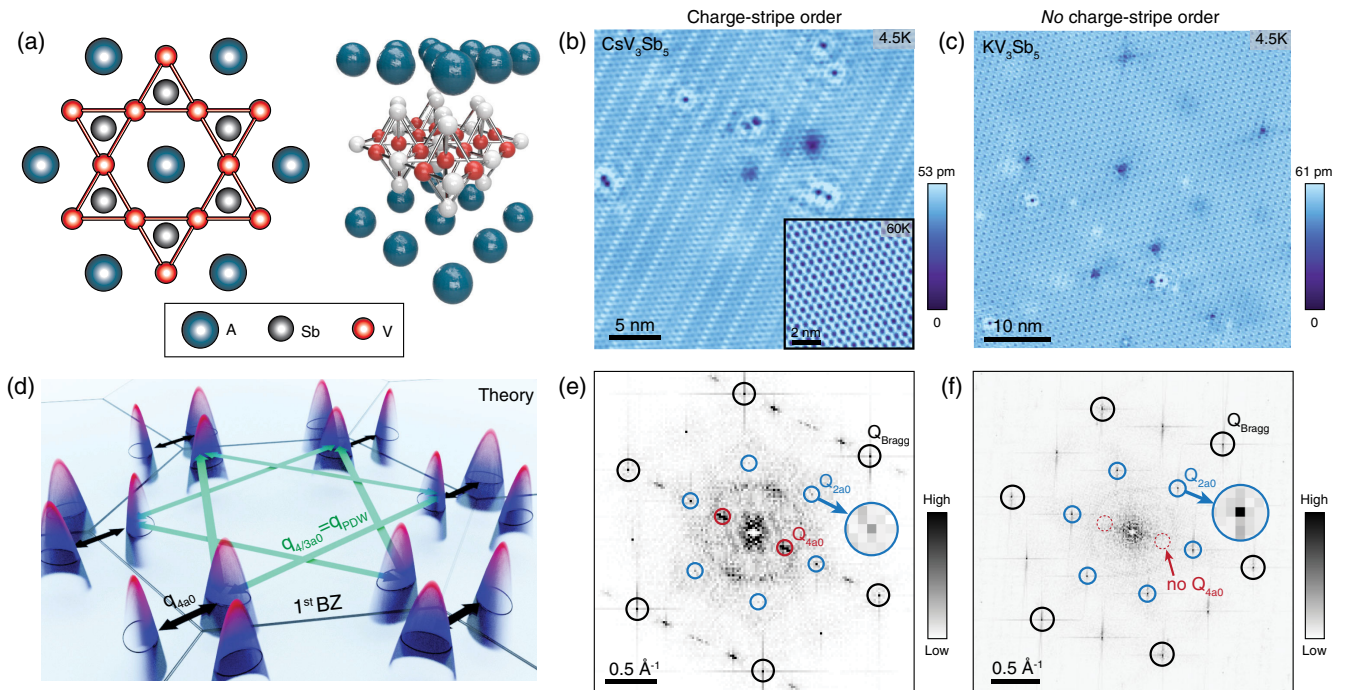


FIG. 1. Crystal structure and emergent charge orders in  $AV_3Sb_5$ . (a) A 2D and a 3D ball model of the crystal structure of  $AV_3Sb_5$  ( $A = K, Cs, Rb$ ) crystals. STM topographs of (b)  $CsV_3Sb_5$  (Sb termination) and (c)  $KV_3Sb_5$  (Sb termination) taken at 4.5 K, and (e, f) their associated Fourier transform (FT). The bottom right inset in panel (b) is a STM topograph encompassing a smaller region of the Sb termination taken at 60 K, the temperature around which the  $4a_0$  charge stripe order disappears. Atomic Bragg peaks  $\mathbf{Q}_{\text{Bragg}}$ ,  $2a_0$  CDW peaks  $\mathbf{Q}_{2a0}$ , and charge-stripe order  $\mathbf{Q}_{4a0}$  peaks in panel (e, f) are circled in black, blue, and red, respectively. (d) Schematic of the theoretically expected Fermi pockets and reciprocal space vectors connecting them from Ref. [15]. For simplicity of visualizing relevant pockets in panel (d), we omit plotting the six additional pockets within the first Brillouin zone, “folded-in” by the  $2a_0$ -by- $2a_0$  CDW. STM setup conditions:  $I_{\text{set}} = 300$  pA,  $V_{\text{sample}} = 50$  mV. Inset:  $I_{\text{set}} = 30$  pA,  $V_{\text{sample}} = 50$  mV (b);  $I_{\text{set}} = 400$  pA,  $V_{\text{sample}} = 20$  mV (c).

resulting in two different types of surfaces: the A termination and the Sb termination [18,19,21,25,26,44]. In STM experiments, we focus on the Sb surface positioned directly above the kagome plane due to its structural stability and the direct access to bulk vanadium-derived kagome bands [19]. Similar to previous experiments [19,25,26,44], STM topographs of the Sb surface of  $\text{CsV}_3\text{Sb}_5$  show a unidirectional electronic modulation related to the  $4a_0$  charge-stripe order [Figs. 1(b) and 1(e)], which forms below about 50–60 K [19]. As more clearly seen from the Fourier transform of the STM topograph at low temperature [Figs. 1(b) and 1(e)], the  $4a_0$  charge order spatially coexists with the  $2a_0$ -by- $2a_0$  charge-density wave [6,34,45].

By replacing Cs with K in an identical  $\text{AV}_3\text{Sb}_5$  crystal structure, the long-range  $4a_0$  charge-stripe order vanishes and cannot be detected on the equivalent Sb surface termination at 4.5 [Figs. 1(c) and 1(f)] [18,21], while most of the other known properties remain qualitatively the same. For example, superconductivity in both materials emerges from the same metallic normal state with a  $2a_0$ -by- $2a_0$  CDW in the kagome plane, which also breaks rotational symmetry of the lattice [18,21,46–48]. In STM measurements, this high-temperature rotation symmetry breaking can be visualized by anisotropic CDW amplitudes [21,46,47], with one preferred direction being markedly different from the other two, which are nearly indistinguishable [insets in Figs. 1(b) and 1(e) in the Supplemental Material [49]]. This symmetry breaking gives rise to three types of domains rotated by 120 degrees from one another, observed by optical birefringence measurements [48]. Muon spin spectroscopy [50,51], magneto-optical Kerr

measurements [48], and circular dichroism [48] have also revealed signatures of time-reversal symmetry breaking in both  $\text{CsV}_3\text{Sb}_5$  and  $\text{KV}_3\text{Sb}_5$ . The two materials provide an exciting playground for the exploration of Fermi surface reconstruction driven by emergent density waves and a fortuitous opportunity to use  $\text{KV}_3\text{Sb}_5$  as a foil for comparison with  $\text{CsV}_3\text{Sb}_5$  to understand the emergence of the charge-stripe order.

We first measure the temperature-dependent Fermi surface and energy-momentum dispersions of  $\text{AV}_3\text{Sb}_5$  using ARPES. While previous experiments investigated the overall renormalization of the Fermi surface driven by the  $2 \times 2$  CDW transition [28,52–55], here we specifically focus on the formation of small Fermi pockets to uncover their renormalization in connection with the emergent density waves using a combination of ARPES and SI-STM. Our ARPES measurements clearly reveal the formation of Fermi pockets, which can be seen in the second Brillouin zone in all  $\text{AV}_3\text{Sb}_5$  systems studied here:  $\text{KV}_3\text{Sb}_5$  [Figs. 2(a)–2(d)],  $\text{CsV}_3\text{Sb}_5$  [Figs. 2(e) and 2(g)] and  $\text{RbV}_3\text{Sb}_5$  [Figs. 2(f) and 2(h)]. Notably, these pockets appear at the  $M_2$  points of the reduced Brillouin zone [blue dashed hexagons in Fig. 2(a)] induced by the  $2 \times 2$  CDW order, and they disappear in the normal state above the CDW transition [Fig. 2(b)]. The ARPES momentum distribution curve (MDC) along the red dashed line in Fig. 2(c) shows the two sides of the Fermi pocket, with a double-peak structure absent in the normal-state MDC [red solid curve in Fig. 2(d)]. The small Fermi pockets are also observed in the  $\text{CsV}_3\text{Sb}_5$  and  $\text{RbV}_3\text{Sb}_5$  variants, indicating that they appear universally in the  $\text{AV}_3\text{Sb}_5$  systems,

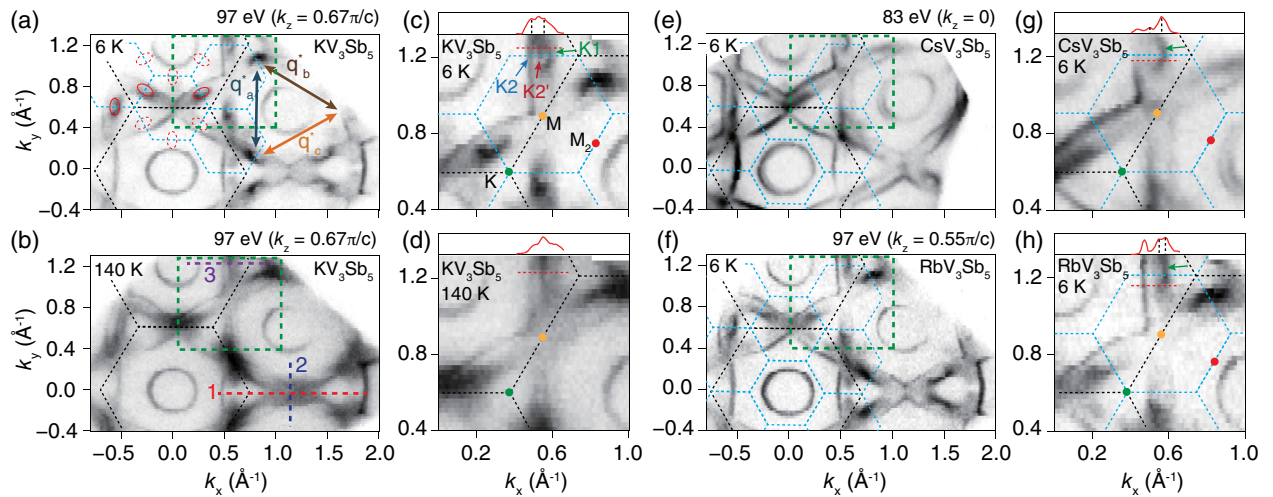


FIG. 2. Momentum-space mapping of Fermi pockets in  $\text{AV}_3\text{Sb}_5$ . Fermi surfaces of  $\text{KV}_3\text{Sb}_5$  across the first and second Brillouin zone at 6 K (a) and 140 K (b). Black and blue dashed hexagons represent the Brillouin zone in normal and charge density wave phases, respectively. Red solid and dashed ellipses indicate the Fermi pockets with strong and weak spectral weights, respectively. The three double-sided arrows with gray, brown, and orange show wave vectors  $\mathbf{q}_a^*$ ,  $\mathbf{q}_b^*$ , and  $\mathbf{q}_c^*$ , respectively. We show Fermi surfaces in the green dashed squares at 6 K (c) and 140 K (d). Green, blue, and red arrows indicate K1, K2, and K2' bands, respectively. Red solid curves represent the momentum distribution curves (MDCs) along the red dashed lines. We show Fermi surfaces of  $\text{CsV}_3\text{Sb}_5$  (e,g) and  $\text{RbV}_3\text{Sb}_5$  (f,h) variants. Green arrows in panels (g) and (h) are visual guides showing the Fermi pockets.

although their spectral weights are comparatively weaker than in  $KV_3Sb_5$  [Figs. 2(e)–2(h)].

Further insights into the formation of small pockets can be obtained by examining the detailed energy-momentum dispersions. Figure 3 summarizes the reconstruction of the electronic structure of  $KV_3Sb_5$ , which displays most clearly the spectral weight associated with the pockets in the CDW state. Consistent with the previous reports [28,52–55], the  $p$ -type van Hove singularities (vHSs) from the K1 and K2 bands are clearly visible in the ARPES spectra above the CDW transition [Figs. 3(c) and 3(d)]. In the CDW state, the main CDW gap of about 80 meV opens at the vHS of the K1 band, forming the “M”-shaped dispersion along the  $\bar{K}$ - $\bar{M}$ - $\bar{K}$  direction [Fig. 3(e)] [28,56]. Importantly, this opening of the CDW gap at the M point drives the reconstruction of the K1 Fermi surface around the  $M_2$  point, resulting in the observed small Fermi pockets [Fig. 3(a)] [55]. We note that along the minor axis, the holelike dispersion is a consequence of the back-folding of the K1 band across the  $M_2$  point [Figs. 3(b) and 3(h)] with the reduced spectral weight of the folded side [see Figs. 2(a) and 2(c)]. In addition, the K2 and K2' bands show clear backbending in the CDW state, suggesting the existence of a CDW gap [red and blue arrows in Fig. 3(h)]. The observed Fermi surface and dispersions are closely

reproduced by DFT calculations of the bulk electronic structure [Figs. 3(a) and 3(b), Sec. IV] [57]. We note that while earlier work reported evidence suggesting the existence of Fermi pockets in  $KV_3Sb_5$  [55], our combination of ARPES and DFT unambiguously demonstrates the formation of small Fermi hole pockets in the CDW state of all  $AV_3Sb_5$  systems, arising from the interplay of vHS and the CDW gap. Moreover, the estimated area of the elliptical pockets (obtained as  $\pi \cdot k_{Fa} \cdot k_{Fb}$ , with  $k_{Fa}$  and  $k_{Fb}$  being the major and the minor radii of the pocket, respectively) found in the present study translates to a quantum oscillation frequency of about  $86.8 \pm 26.2$  T via the Onsager relation, in agreement with recent quantum oscillation studies within the experimental resolution (Table 1 in the Supplemental Material [49]). The quantitative correspondence between the ARPES and quantum oscillation experiments further confirms the bulk nature of the observed Fermi pockets.

Complementary to ARPES measurements of the electronic band structure in the normal state, we image the scattering and interference of electrons using SI-STM. Fourier transforms of  $dI/dV(\mathbf{r}, V)$  maps on the Sb surface of the two systems display similar, dispersive scattering wave vectors  $\mathbf{q}_1$  and  $\mathbf{q}_2$  (Figs. 1 and 2 in the Supplemental Material [49]). In addition to these previously reported wave vectors, our high-resolution SI-STM measurements

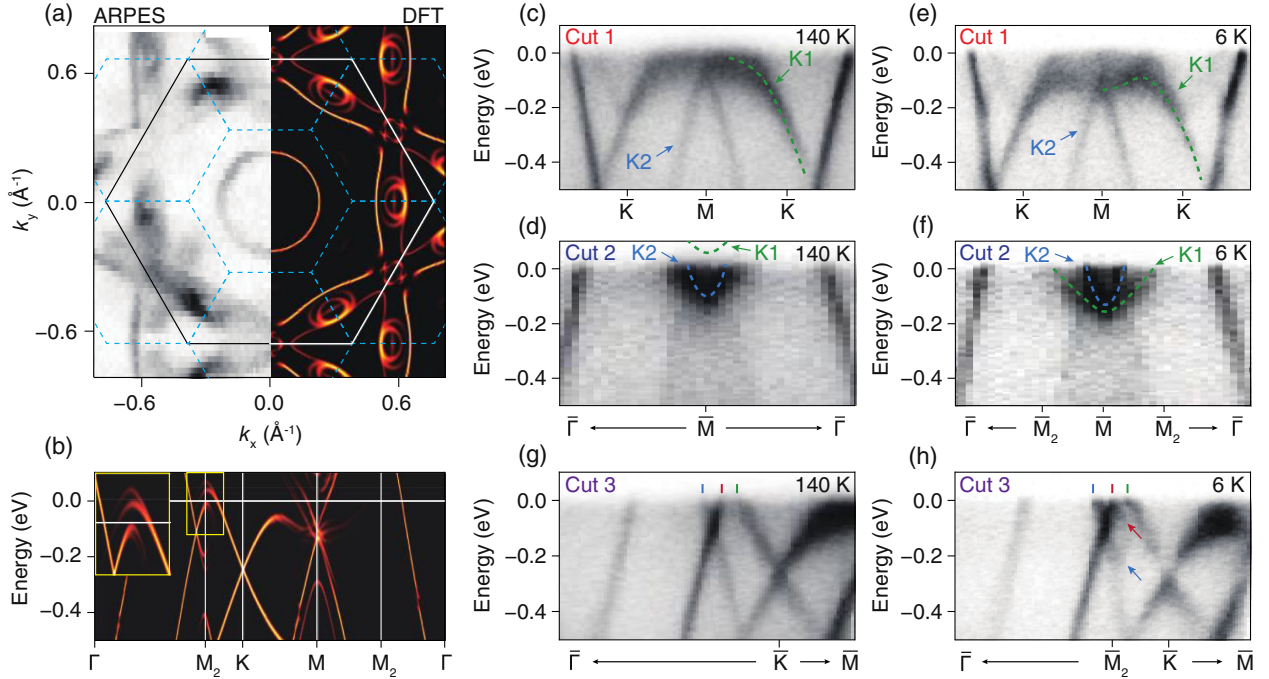


FIG. 3. Reconstruction of the electronic structure across the CDW transition in  $KV_3Sb_5$ . (a) Comparison between experimental and calculated Fermi surfaces at 97 eV ( $k_z = 0.67\pi/c$ ). The calculated Fermi surface assumes a staggered tri-hexagonal charge order and is threefold symmetrized to average over three symmetry-equivalent domains. (b) Calculated dispersion along high-symmetry points for  $k_z = 0.67\pi/c$ . The inset shows the magnified band dispersion inside the yellow box. We show the energy-momentum dispersion along  $\bar{K}$ - $\bar{M}$ - $\bar{K}$  [red dashed line in Fig. 2(b)] at 140 K (c) and 6 K (e),  $\bar{\Gamma}$ - $\bar{M}$ - $\bar{\Gamma}$  [navy dashed line in Fig. 2(b)] at 140 K (d) and 6 K (f), and  $\bar{\Gamma}$ - $\bar{M}_2$ - $\bar{K}$ - $\bar{M}$  [purple dashed line in Fig. 2(b)] at 140 K (g) and 6 K (h). The K1 and K2 bands (marked with green and blue arrows, respectively) exhibit a holelike dispersion along the  $\bar{K}$ - $\bar{M}$ - $\bar{K}$  direction (c) and electronlike dispersion along  $\bar{\Gamma}$ - $\bar{M}$ - $\bar{\Gamma}$  (d).

reveal a set of new, dispersive scattering wave vectors  $\mathbf{q}_i^*$ , where  $i = a, b, \text{ or } c$  lattice directions [Fig. 4(a)]. For simplicity, we first examine  $\mathbf{q}_i^*$  in  $\text{KV}_3\text{Sb}_5$ , in the absence of  $4a_0$  charge-stripe ordering. In contrast to  $\mathbf{q}_2$  scattering wave vectors that are markedly unidirectional (Fig. 1 in the Supplemental Material [49]),  $\mathbf{q}_i^*$  wave vectors appear along all three atomic Bragg peak  $\mathbf{Q}_{\text{Bragg}}^i$  directions [Figs. 4(a) and 4(b)]. They are detectable around the Fermi level and disperse with energy in a similar manner along the three lattice directions [Figs. 4(d)–4(f), and 3 in the Supplemental Material [49]]. The dispersive nature of  $\mathbf{q}_i^*$  suggests that these wave vectors originate from scattering between different points on the constant energy contour, which changes concomitantly with the band structure evolution. The magnitude of  $\mathbf{q}_i^*$  from SI-STM measurements is beautifully consistent with the pockets extracted from ARPES (Fig. 4 in the Supplemental Material [49]). The scattering primarily occurs between the outer sides of the pockets with a significantly larger spectral weight, as

observed in ARPES measurements (Figs. 4 and 5 in the Supplemental Material [49]). We stress that the observed small pockets correspond to residual electronic states near the Fermi level after band folding and gapping induced by the  $2 \times 2$  CDW state in the kagome plane. Taken together, our data demonstrate an intimate relationship between the emergence of  $\mathbf{q}_i^*$  and the existence of Fermi pockets near the reduced Brillouin zone boundary [Fig. 4(c)]. We note that there is a slight difference in the dispersion of  $\mathbf{q}_a^*$  compared to the other two vectors in Figs. 4(d)–4(f). This difference may be due to the overall  $C_2$ -symmetric band structure in the rotation symmetry broken state that maintains an in-plane reflection symmetry along the  $\mathbf{q}_a^*$  direction while the other two are broken (Fig. 1 in the Supplemental Material [49]) [21,47], or it could possibly be due to anisotropic electron-phonon coupling [58].

Interestingly, the morphology of  $\mathbf{q}_i^*$  changes profoundly as the charge-stripe order forms in  $\text{CsV}_3\text{Sb}_5$ . While  $\mathbf{q}_b^*$  and  $\mathbf{q}_c^*$  are still present and disperse with energy, we no longer

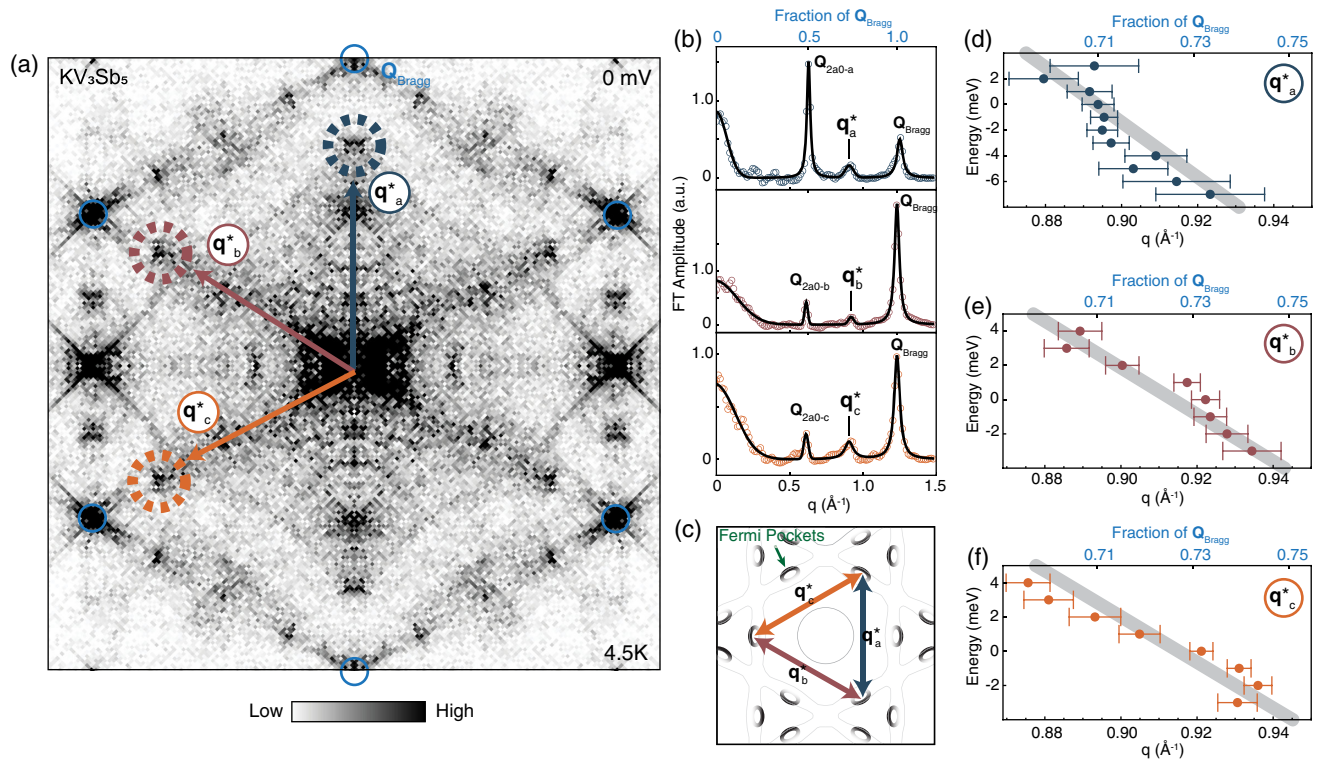


FIG. 4. Dispersive scattering peaks  $\mathbf{q}^*$  near the Fermi level in  $\text{KV}_3\text{Sb}_5$ . (a) Twofold symmetrized FT of  $dI/dV(\mathbf{r}, V = 0 \text{ mV})$  map acquired on the Sb surface of  $\text{KV}_3\text{Sb}_5$ . Atomic Bragg peaks  $\mathbf{Q}_{\text{Bragg}}$  are enclosed in dark blue circles, while the new scattering peaks  $\mathbf{q}_i^*$  ( $i = a, b, \text{ or } c$ ) near  $3/4 \cdot \mathbf{Q}_{\text{Bragg}}$  are shown by dashed circles in gray ( $\mathbf{q}_a^*$ ), brown ( $\mathbf{q}_b^*$ ), and orange ( $\mathbf{q}_c^*$ ). (b) FT linecuts along the three  $\mathbf{Q}_{\text{Bragg}}$  directions (circles) and the Gaussian fittings to each peak in the curve (solid line). The linecut is averaged by seven pixels perpendicular to the linecut. (c) Approximate schematic of the relevant portions of the Fermi surface of the  $\text{KV}_3\text{Sb}_5$  band structure, with an example of a Fermi pocket shown by the green arrow. The three double-sided arrows in panel (c) denote scattering processes corresponding to different  $\mathbf{q}^*$  wave vectors in panel (a). In principle, other scattering vectors between the pockets should be possible, in addition to  $\mathbf{q}_i^*$ , but we are not able to clearly resolve them in our data (Fig. 9 in the Supplemental Material [49]). (d)–(f) Position of the  $\mathbf{q}_i^*$  peaks as a function of energy. All three peaks are dispersive with similar band velocities [the thick gray line in panels (d)–(f) is a visual guide]. The position of the peak is extracted from Gaussian fitting as shown for one energy in panel (b), and the error bars represent the standard error from Gaussian fitting. STM setup conditions: (a)  $I_{\text{set}} = 400 \text{ pA}$ ,  $V_{\text{sample}} = 20 \text{ mV}$ ,  $V_{\text{exc}} = 1 \text{ mV}$ ,  $4.5 \text{ K}$ .

observe a dispersive wave vector along the third direction [Figs. 5(a) and 5(b)]. Instead, we only detect a non-dispersive peak [Fig. 5(b), top panel] in the vicinity. As  $\mathbf{q}_i^*$  represents the fingerprint of scattering between the small pockets, the change in  $\mathbf{q}_a^*$  is directly tied to the additional renormalization of the hole pockets, which in turn accompanies the emergence of the charge-stripe order. A possible schematic of the charge-stripe-order-driven modification of the constant energy contour is shown in Fig. 5(c), where the size and the shape of the pockets connected by the  $\mathbf{Q}_{4a_0}$  wave vector change. Another intriguing aspect of this band-structure change is that  $\mathbf{q}_b^*$  and  $\mathbf{q}_c^*$  now bend away from the high-symmetry  $\Gamma$ -M directions [Figs. 5(e) and 5(f)]. We note that this is not the case for the equivalent vectors when the  $4a_0$  charge order is absent (Fig. 6 in the Supplemental Material [49]). This deviation of  $\mathbf{q}_b^*$  and

$\mathbf{q}_c^*$  from high-symmetry directions demonstrates additional renormalization of the Fermi surface.

The measurements above explored the effects of density waves in the normal state. In the superconducting state of  $\text{CsV}_3\text{Sb}_5$ , the superconducting gap and the coherence peak height also vary spatially in a periodic manner, as reported in a previous experiment [25]. Such modulations are a hallmark of a Cooper pair density wave phase. The period of the emergent pair density wave in  $\text{CsV}_3\text{Sb}_5$  is about  $4a_0/3$ -by- $4a_0/3$  in plane, and it coexists with the  $4a_0$  charge stripes and the  $2a_0$ -by- $2a_0$  CDW [25]. Interestingly, the  $4a_0/3$ -by- $4a_0/3$  modulation in real space translates to about  $0.75 \mathbf{Q}_{\text{Bragg}}$  in reciprocal space, which is exactly the same magnitude and direction of  $\mathbf{q}^*$  reciprocal-space wave vectors uncovered here. As such, our work also sheds light on the spectroscopic origin of the pair density wave related

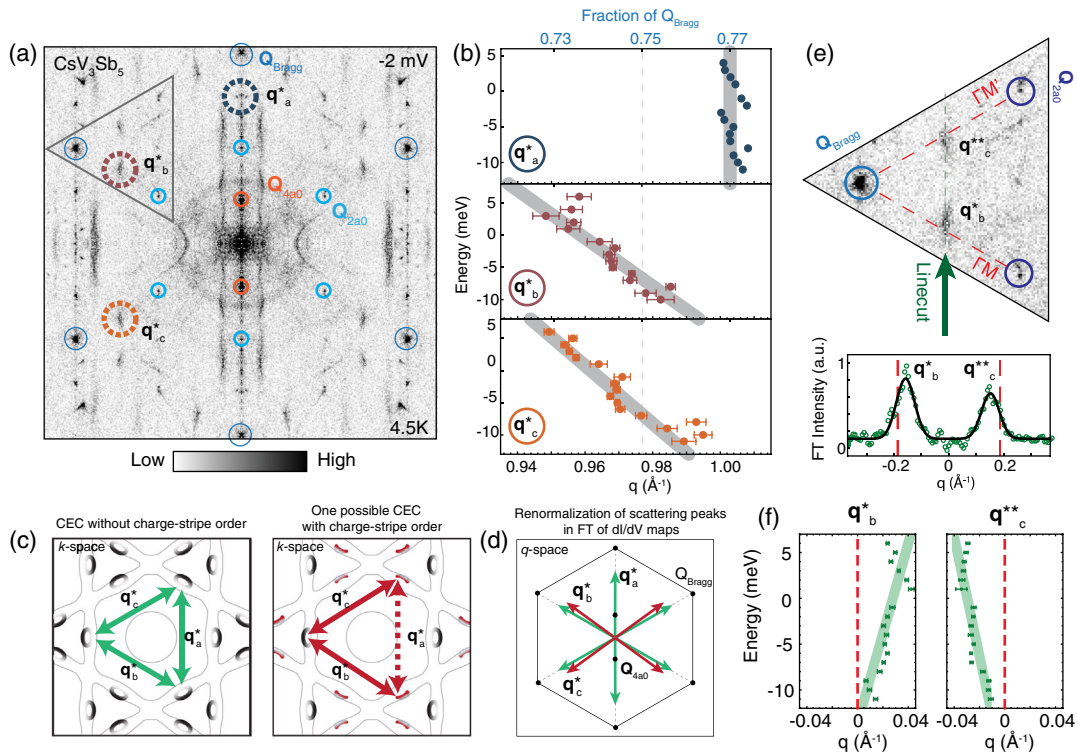


FIG. 5. Renormalization of  $\mathbf{q}^*$  scattering wave vectors in the presence of the charge-stripe order in  $\text{CsV}_3\text{Sb}_5$ . (a) FT of the  $dI/dV(\mathbf{r}, V = -2 \text{ mV})$  map acquired over a 96-nm-square Sb surface of  $\text{CsV}_3\text{Sb}_5$ . Atomic Bragg peaks  $\mathbf{Q}_{\text{Bragg}}$  are enclosed in blue circles, while the new scattering peaks  $\mathbf{q}_i^*$  ( $i = a, b, \text{ or } c$ ) are shown by dashed circles in dark gray ( $\mathbf{q}_a^*$ ), brown ( $\mathbf{q}_b^*$ ), and orange ( $\mathbf{q}_c^*$ ). (b) Dispersion of the  $\mathbf{q}_i^*$  peaks as a function of energy. In contrast to the dispersion of  $\mathbf{q}_i^*$  in the absence of charge-stripe order in Fig. 3, only  $\mathbf{q}_b^*$  and  $\mathbf{q}_c^*$  are dispersive, while  $\mathbf{q}_a^*$  is static and at a slightly different  $q$ -space position. (c) Approximate schematic of the Fermi surface of  $\text{CsV}_3\text{Sb}_5$  without (left panel) and with (right panel) charge-stripe order. (d) Comparison of  $\mathbf{q}_i^*$  scattering wave vectors seen in our experiments, consistent with the schematics in panel (c). (e) Zoom on a region in FT space [denoted by a triangle in panel (a)], more clearly showing  $\mathbf{q}_b^*$  and the Bragg reflection of  $\mathbf{q}_c^*$  (labeled  $\mathbf{q}_c^{**}$ ). The red dashed line connects  $\mathbf{Q}_{\text{Bragg}}$  (blue circle) and  $\mathbf{Q}_{2a_0}$  (purple circle). The bottom curve in panel (e) is the linecut (green open circles) taken along the green arrow direction in the top panel, and Gaussian fits (solid black line). The linecut is averaged by three pixels along the linecut and 15 pixels perpendicular to the linecut. (f) Positions of the  $\mathbf{q}_b^*$  and  $\mathbf{q}_c^{**}$  in panel (e) relative to the high-symmetry line at each energy for  $\text{CsV}_3\text{Sb}_5$  (vertical red dashed line). The position of the peak at each energy is extracted from Gaussian fits as seen in the example in panel (e). The error bars represent the standard error from Gaussian fitting. STM setup conditions: (a)  $I_{\text{set}} = 40 \text{ pA}$ ,  $V_{\text{sample}} = -2 \text{ mV}$ ,  $V_{\text{exc}} = 1 \text{ mV}$ ,  $4.5 \text{ K}$ .

to the same Fermi pockets [see schematic in Fig. 1(d)] originally formed by band folding in the  $2a_0$ -by- $2a_0$  CDW state.

### III. DISCUSSION

The difficulty of pinpointing spectroscopic origins of the  $4a_0$  charge-stripe order thus far and its apparent absence in x-ray diffraction experiments prompted a hypothesis that the charge-stripe order may be a surface reconstruction [38]. Our data reveal how the formation of the  $4a_0$  charge order accompanies the renormalization of the electronic band structure tied to small hole pockets that are intrinsic parts of the bulk electronic band structure. This, in turn, highlights charge-stripe ordering as an inherent feature that can be realized in this family of kagome superconductors. It was theoretically proposed that favorably positioned Fermi pockets could drive the emergence of the  $4a_0$  charge order [15] [Fig. 1(d)]. The combination of our ARPES and STM data suggests that such a condition may indeed be satisfied. Further supporting the notion that unidirectional charge ordering can be realized in kagome superconductors, we note that recent scattering measurements unveiled signatures of unidirectional bulk charge correlations in doped  $\text{CsV}_3\text{Sb}_5$  [59]. We also mention that the sole presence of these Fermi pockets is not sufficient to drive the formation of the charge stripe order in all  $\text{AV}_3\text{Sb}_5$  members, as  $\mathbf{q}^*$  is still present in  $\text{KV}_3\text{Sb}_5$  (Fig. 3), although no long-range charge-stripe order is detected in STM measurements [18,21]. By methodical STM investigation of different  $\text{KV}_3\text{Sb}_5$  crystals and different regions of the sample, we find that short-range charge-stripe order can be found in three out of 18 samples (Fig. 8 in the Supplemental Material [49]). This finding demonstrates that  $\text{KV}_3\text{Sb}_5$  may be at the cusp of forming a static long-range charge-stripe order, similarly to the Cs and Rb variants. Given that K atoms are smaller than Cs or Rb, it is conceivable that microscopic details of the particular system also play a role in the formation of the charge-stripe order, in addition to the existence of underlying small pockets connected by the  $4a_0$  wave vector. It will be of interest to explore if the pair density wave also emerges in the superconducting state of  $\text{KV}_3\text{Sb}_5$ . Future experimental and theoretical work will be necessary to fully understand the physical mechanism needed to drive these phenomena.

It is worth noting that recent termination-resolved ARPES experiments on  $\text{CsV}_3\text{Sb}_5$  reported that only alkali-metal-terminated surfaces exhibit a clear reconstruction of the ARPES spectra in the CDW state [60]. In contrast, ARPES spectra from the Sb-terminated surface do not show band dispersion variations across the CDW transition, which is understood to be due to suppression of the CDW order caused by the hole-rich nature of the Sb surface [60]. Based on these results, we conclude that the present ARPES spectra were obtained from the K-terminated surface. Interestingly, contrary to the ARPES

side, STM results have clearly identified the presence of the  $2 \times 2$  charge modulation in both alkali-metal- and Sb-terminated surfaces [26]. Moreover, temperature-dependent tunneling spectra clearly reveal the CDW gap at the Fermi level with a 40-meV energy scale on the Sb-terminated surface [19,26], consistent with the energy scale of the CDW gap at the Fermi level observed by ARPES [28]. These results demonstrate that bulk charge order persists even on the Sb-terminated surface, and they allow us to establish a valid connection between the STM and ARPES results obtained from Sb and alkali metal surfaces, respectively.

The intriguing renormalization of the Fermi surface in  $\text{CsV}_3\text{Sb}_5$  in the presence of charge-stripe order suggests that a subset of Fermi pockets is reconstructed in reciprocal space. It is conceivable that this, in turn, may explain some low frequencies in quantum oscillation experiments that are difficult to capture by a theoretical model that only takes into account the  $2a_0 \times 2a_0$  CDW in the kagome plane. We note that the inevitable presence of charge-stripe domains of submicron scales [19] hinders the observation of the additional renormalization of pockets by ARPES, as it averages over larger regions of the sample likely spanning stripe domains oriented along all three lattice directions. Shubnikov–de Hass [35,40] and de Haas–van Alphen [42] quantum oscillation experiments have detected many low-frequency orbits, several of which carry a nontrivial Berry phase [40,42]. The pockets observed here are due to Fermi surface reconstruction and could acquire concentrated Berry curvature and orbital magnetic moments if time-reversal symmetry is broken in the CDW state [15]. As a result, these pockets may be tunable by a magnetic field, which could be explored in future field-sensitive experiments.

### IV. METHODS

*Single crystal growth.*—Bulk single crystals of  $\text{CsV}_3\text{Sb}_5$  and  $\text{KV}_3\text{Sb}_5$  were grown and characterized as described in Refs. [6,8].

*ARPES measurements.*—ARPES experiments were performed at Beamline 7.0.2 of the Advanced Light Source (MAESTRO). The photoelectrons were collected by a hemispherical electron analyzer equipped with a deflector (DA30, Scienta Omicron).  $\text{KV}_3\text{Sb}_5$ ,  $\text{RbV}_3\text{Sb}_5$ ,  $\text{CsV}_3\text{Sb}_5$ , and Sn-doped  $\text{CsV}_3\text{Sb}_5$  single crystals were cleaved inside an ultra-high-vacuum (UHV) ARPES chamber ( $\sim 4 \times 10^{-11}$  torr). The energy and momentum resolutions were better than 20 meV and  $0.01 \text{ \AA}^{-1}$ .

*STM measurements.*—STM data were acquired using a customized Unisoku USM1300 microscope at the base temperature of 4.5 K and zero magnetic field. We cleaved each sample at a cryogenic temperature and immediately inserted it into the STM head held at 4.5 K [19,21,47]. Spectroscopic measurements were made using a standard lock-in technique with 915-Hz frequency and bias

excitation as noted in the figure captions. STM tips used were homemade, chemically etched, tungsten tips, annealed in a UHV chamber to a bright orange color before STM experiments. We applied the Lawler-Fujita drift-correction algorithm to all our data to align the atomic Bragg peaks onto single pixels with coordinates that are even integers.

*Density functional theory calculations.*—Electronic structure calculations were performed using the Vienna *ab initio* simulation (VASP) package [61,62] based on the projector augmented wave (PAW) potentials [63,64] and the Perdew-Burke-Ernzerhof (PBE) exchange-correlation functional [65]. Effective tight-binding Hamiltonians projected using the Wannier90 code [66] were derived to unfold the band structure in the CDW state [67].

### ACKNOWLEDGMENTS

I. Z. gratefully acknowledges support from NSF-DMR 2216080 for STM experiments. Work at M. I. T. was supported by the Air Force Office of Scientific Research Young Investigator Program under Grant No. FA9550-19-1-0063 and by the STC Center for Integrated Quantum Materials (National Science Foundation Grant No. DMR-1231319). This research used resources of the Advanced Light Source, a U.S. Department of Energy Office of Science User Facility under Contract No. DE-AC02-05CH11231. M. K. acknowledges a Samsung Scholarship from the Samsung Foundation of Culture. Z. W. acknowledges the support of U.S. Department of Energy, Basic Energy Sciences Grant No. DE-FG02-99ER45747 and the Cottrell SEED Award No. 27856 from the Research Corporation for Science Advancement. The theoretical calculations were funded, in part, by the Gordon and Betty Moore Foundation EPIQS Initiative, Grant No. GBMF9070 to J. G. C. S. D. W. and B. R. O. gratefully acknowledge support via the UC Santa Barbara NSF Quantum Foundry funded via the Q-AMASE-i program under Award No. DMR-1906325.

---

[1] N. Doiron-Leyraud, C. Proust, D. LeBoeuf, J. Levallois, J.-B. Bonnemaïson, R. Liang, D. A. Bonn, W. N. Hardy, and L. Taillefer, *Quantum Oscillations and the Fermi Surface in an Underdoped High- $T_c$  Superconductor*, *Nature (London)* **447**, 565 (2007).

[2] J. Meng *et al.*, *Coexistence of Fermi Arcs and Fermi Pockets in a High- $T_c$  Copper Oxide Superconductor*, *Nature (London)* **462**, 335 (2009).

[3] P. D. C. King *et al.*, *Structural Origin of Apparent Fermi Surface Pockets in Angle-Resolved Photoemission of  $\text{Bi}_2\text{Sr}_{2-x}\text{La}_x\text{CuO}_{6+\delta}$* , *Phys. Rev. Lett.* **106**, 127005 (2011).

[4] S. Kunisada *et al.*, *Observation of Small Fermi Pockets Protected by Clean  $\text{CuO}_2$  Sheets of a High- $T_c$  Superconductor*, *Science* **369**, 833 (2020).

[5] B. R. Ortiz *et al.*, *New Kagome Prototype Materials: Discovery of  $\text{KV}_3\text{Sb}_5\text{RbV}_3\text{Sb}_5$  and  $\text{CsV}_3\text{Sb}_5$* , *Phys. Rev. Mater.* **3**, 094407 (2019).

[6] B. R. Ortiz *et al.*,  *$\text{CsV}_3\text{Sb}_5$ : A  $Z_2$  Topological Kagome Metal with a Superconducting Ground State*, *Phys. Rev. Lett.* **125**, 247002 (2020).

[7] Q. Yin, Z. Tu, C. Gong, Y. Fu, S. Yan, and H. Lei, *Superconductivity and Normal-State Properties of Kagome Metal  $\text{RbV}_3\text{Sb}_5$  Single Crystals*, *Chin. Phys. Lett.* **38**, 037403 (2021).

[8] B. R. Ortiz, P. M. Sarte, E. M. Kenney, M. J. Graf, S. M. L. Teicher, R. Seshadri, and S. D. Wilson, *Superconductivity in the  $Z_2$  Kagome Metal  $\text{KV}_3\text{Sb}_5$* , *Phys. Rev. Mater.* **5**, 034801 (2021).

[9] X. Feng, K. Jiang, Z. Wang, and J. Hu, *Chiral Flux Phase in the Kagome Superconductor  $\text{AV}_3\text{Sb}_5$* , *Sci. Bull.* **66**, 1384 (2021).

[10] H. Tan, Y. Liu, Z. Wang, and B. Yan, *Charge Density Waves and Electronic Properties of Superconducting Kagome Metals*, *Phys. Rev. Lett.* **127**, 046401 (2021).

[11] M. M. Denner, R. Thomale, and T. Neupert, *Analysis of Charge Order in the Kagome Metal  $\text{AV}_3\text{Sb}_5$  ( $A = \text{K}, \text{Rb}, \text{Cs}$ )*, *Phys. Rev. Lett.* **127**, 217601 (2021).

[12] Y.-P. Lin and R. M. Nandkishore, *Complex Charge Density Waves at Van Hove Singularity on Hexagonal Lattices: Haldane-Model Phase Diagram and Potential Realization in the Kagome Metals  $\text{AV}_3\text{Sb}_5$  ( $A = \text{K}, \text{Rb}, \text{Cs}$ )*, *Phys. Rev. B* **104**, 045122 (2021).

[13] T. Park, M. Ye, and L. Balents, *Electronic Instabilities of Kagome Metals: Saddle Points and Landau Theory*, *Phys. Rev. B* **104**, 035142 (2021).

[14] M. H. Christensen, T. Birol, B. M. Andersen, and R. M. Fernandes, *Theory of the Charge Density Wave in  $\text{AV}_3\text{Sb}_5$  Kagome Metals*, *Phys. Rev. B* **104**, 214513 (2021).

[15] S. Zhou and Z. Wang, *Chern Fermi Pocket, Topological Pair Density Wave, and Charge-4e and Charge-6e Superconductivity in Kagome Superconductors*, *Nat. Commun.* **13**, 7288 (2022).

[16] M. H. Christensen, T. Birol, B. M. Andersen, and R. M. Fernandes, *Loop Currents in  $\text{AV}_3\text{Sb}_5$  Kagome Metals: Multipolar and Toroidal Magnetic Orders*, *Phys. Rev. B* **106**, 144504 (2022).

[17] T. Schwemmer *et al.*, *Pair Density Wave Instability in the Kagome Hubbard Model*, arXiv:2302.08517.

[18] Y.-X. Jiang *et al.*, *Unconventional Chiral Charge Order in Kagome Superconductor  $\text{KV}_3\text{Sb}_5$* , *Nat. Mater.* **20**, 1353 (2021).

[19] H. Zhao, H. Li, B. R. Ortiz, S. M. L. Teicher, T. Park, M. Ye, Z. Wang, L. Balents, S. D. Wilson, and I. Zeljkovic, *Cascade of Correlated Electron States in the Kagome Superconductor  $\text{CsV}_3\text{Sb}_5$* , *Nature (London)* **599**, 216 (2021).

[20] T. Qian, M. H. Christensen, C. Hu, A. Saha, B. M. Andersen, R. M. Fernandes, T. Birol, and N. Ni, *Revealing the Competition between Charge Density Wave and Superconductivity  $\text{CsV}_3\text{Sb}_5$  through Uniaxial Strain*, *Phys. Rev. B* **104**, 144506 (2021).

[21] H. Li, H. Zhao, B. R. Ortiz, T. Park, M. Ye, L. Balents, Z. Wang, S. D. Wilson, and I. Zeljkovic, *Rotation Symmetry*



- Breaking in the Normal State of a Kagome Superconductor*  $\text{KV}_3\text{Sb}_5$ , *Nat. Phys.* **18**, 265 (2022).
- [22] C. Guo *et al.*, *Switchable Chiral Transport in Charge-Ordered Kagome Metal*  $\text{CsV}_3\text{Sb}_5$ , *Nature (London)* **611**, 461 (2022).
- [23] Q. Wu *et al.*, *Simultaneous Formation of Two-Fold Rotation Symmetry with Charge Order in the Kagome Superconductor*  $\text{CsV}_3\text{Sb}_5$  by Optical Polarization Rotation Measurement, *Phys. Rev. B* **106**, 205109 (2022).
- [24] A. Ptok, A. Kobińska, M. Sternik, J. Łażewski, P. T. Jochym, A. M. Oleś, and P. Piekarczyk, *Dynamical Study of the Origin of the Charge Density Wave in*  $\text{AV}_3\text{Sb}_5$  ( $A = \text{K}, \text{Rb}, \text{Cs}$ ) Compounds, *Phys. Rev. B* **105**, 235134 (2022).
- [25] H. Chen *et al.*, *Roton Pair Density Wave in a Strong-Coupling Kagome Superconductor*, *Nature (London)* **599**, 222 (2021).
- [26] Z. Liang *et al.*, *Three-Dimensional Charge Density Wave and Surface-Dependent Vortex-Core States in a Kagome Superconductor*  $\text{CsV}_3\text{Sb}_5$ , *Phys. Rev. X* **11**, 031026 (2021).
- [27] H. Li *et al.*, *Observation of Unconventional Charge Density Wave without Acoustic Phonon Anomaly in Kagome Superconductors*  $\text{AV}_3\text{Sb}_5$  ( $A = \text{Rb}, \text{Cs}$ ), *Phys. Rev. X* **11**, 031050 (2021).
- [28] M. Kang *et al.*, *Twofold van Hove Singularity and Origin of Charge Order in Topological Kagome Superconductor*  $\text{CsV}_3\text{Sb}_5$ , *Nat. Phys.* **18**, 301 (2022).
- [29] Y. Xiang, Q. Li, Y. Li, W. Xie, H. Yang, Z. Wang, Y. Yao, and H.-H. Wen, *Twofold Symmetry of  $c$ -Axis Resistivity in Topological Kagome Superconductor*  $\text{CsV}_3\text{Sb}_5$  with In-Plane Rotating Magnetic Field, *Nat. Commun.* **12**, 6727 (2021).
- [30] S.-Y. Yang *et al.*, *Giant, Unconventional Anomalous Hall Effect in the Metallic Frustrated Magnet Candidate*,  $\text{KV}_3\text{Sb}_5$ , *Sci. Adv.* **6**, eabb6003 (2020).
- [31] H.-S. Xu, Y.-J. Yan, R. Yin, W. Xia, S. Fang, Z. Chen, Y. Li, W. Yang, Y. Guo, and D.-L. Feng, *Multiband Superconductivity with Sign-Preserving Order Parameter in Kagome Superconductor*  $\text{CsV}_3\text{Sb}_5$ , *Phys. Rev. Lett.* **127**, 187004 (2021).
- [32] E. Uykur, B. R. Ortiz, S. D. Wilson, M. Dressel, and A. A. Tsirlin, *Optical Detection of the Density-Wave Instability in the Kagome Metal*  $\text{KV}_3\text{Sb}_5$ , *npj Quantum Mater.* **7**, 16 (2022).
- [33] X. Zhou, Y. Li, X. Fan, J. Hao, Y. Dai, Z. Wang, Y. Yao, and H.-H. Wen, *Origin of Charge Density Wave in the Kagome Metal*  $\text{CsV}_3\text{Sb}_5$  as Revealed by Optical Spectroscopy, *Phys. Rev. B* **104**, L041101 (2021).
- [34] Y. M. Oey, B. R. Ortiz, F. Kaboudvand, J. Frassinetti, E. Garcia, R. Cong, S. Sanna, V. F. Mitrović, R. Seshadri, and S. D. Wilson, *Fermi Level Tuning and Double-Dome Superconductivity in the Kagome Metal*  $\text{CsV}_3\text{Sb}_{5-x}\text{Sn}_x$ , *Phys. Rev. Mater.* **6**, L041801 (2022).
- [35] B. R. Ortiz, S. M. L. Teicher, L. Kautzsch, P. M. Sarte, N. Ratcliff, J. Harter, J. P. C. Ruff, R. Seshadri, and S. D. Wilson, *Fermi Surface Mapping and the Nature of Charge-Density-Wave Order in the Kagome Superconductor*  $\text{CsV}_3\text{Sb}_5$ , *Phys. Rev. X* **11**, 041030 (2021).
- [36] F. H. Yu, T. Wu, Z. Y. Wang, B. Lei, W. Z. Zhuo, J. J. Ying, and X. H. Chen, *Concurrence of Anomalous Hall Effect and Charge Density Wave in a Superconducting Topological Kagome Metal*, *Phys. Rev. B* **104**, L041103 (2021).
- [37] M. L. Kiesel, C. Platt, and R. Thomale, *Unconventional Fermi Surface Instabilities in the Kagome Hubbard Model*, *Phys. Rev. Lett.* **110**, 126405 (2013).
- [38] H. Li *et al.*, *Discovery of Conjoined Charge Density Waves in the Kagome Superconductor*  $\text{CsV}_3\text{Sb}_5$ , *Nat. Commun.* **13**, 6348 (2022).
- [39] T. Neupert, M. M. Denner, J.-X. Yin, R. Thomale, and M. Z. Hasan, *Charge Order and Superconductivity in Kagome Materials*, *Nat. Phys.* **18**, 137 (2022).
- [40] Y. Fu *et al.*, *Quantum Transport Evidence of Topological Band Structures of Kagome Superconductor*  $\text{CsV}_3\text{Sb}_5$ , *Phys. Rev. Lett.* **127**, 207002 (2021).
- [41] X. Huang, C. Guo, C. Putzke, M. Gutierrez-Amigo, Y. Sun, M. G. Vergniory, I. Errea, D. Chen, C. Felser, and P. J. W. Moll, *Three-Dimensional Fermi Surfaces from Charge Order in Layered*  $\text{CsV}_3\text{Sb}_5$ , *Phys. Rev. B* **106**, 064510 (2022).
- [42] K. Shrestha *et al.*, *Nontrivial Fermi Surface Topology of the Kagome Superconductor*  $\text{CsV}_3\text{Sb}_5$  Probed by de Haas-van Alphen Oscillations, *Phys. Rev. B* **105**, 024508 (2022).
- [43] C. Broyles, D. Graf, H. Yang, X. Dong, H. Gao, and S. Ran, *Effect of the Interlayer Ordering on the Fermi Surface of Kagome Superconductor*  $\text{CsV}_3\text{Sb}_5$  Revealed by Quantum Oscillations, *Phys. Rev. Lett.* **129**, 157001 (2022).
- [44] Q. Wang *et al.*, *Charge Density Wave Orders and Enhanced Superconductivity under Pressure in the Kagome Metal*  $\text{CsV}_3\text{Sb}_5$ , *Adv. Mater.* **33**, 2102813 (2021).
- [45] Z. Zhang *et al.*, *Pressure-Induced Reemergence of Superconductivity in the Topological Kagome Metal*  $\text{CsV}_3\text{Sb}_5$ , *Phys. Rev. B* **103**, 224513 (2021).
- [46] L. Nie *et al.*, *Charge-Density-Wave-Driven Electronic Nematicity in a Kagome Superconductor*, *Nature (London)* **604**, 59 (2022).
- [47] H. Li, H. Zhao, B. R. Ortiz, Y. Oey, Z. Wang, S. D. Wilson, and I. Zeljkovic, *Unidirectional Coherent Quasiparticles in the High-Temperature Rotational Symmetry Broken Phase of*  $\text{AV}_3\text{Sb}_5$  Kagome Superconductors, *Nat. Phys.* **19**, 637 (2023).
- [48] Y. Xu, Z. Ni, Y. Liu, B. R. Ortiz, Q. Deng, S. D. Wilson, B. Yan, L. Balents, and L. Wu, *Three-State Nematicity and Magneto-Optical Kerr Effect in the Charge Density Waves in Kagome Superconductors*, *Nat. Phys.* **18**, 1470 (2022).
- [49] See Supplemental Material at <http://link.aps.org/supplemental/10.1103/PhysRevX.13.031030> for [brief description].
- [50] C. Mielke *et al.*, *Time-Reversal Symmetry-Breaking Charge Order in a Kagome Superconductor*, *Nature (London)* **602**, 245 (2022).
- [51] R. Khasanov *et al.*, *Time-Reversal Symmetry Broken by Charge Order in*  $\text{CsV}_3\text{Sb}_5$ , *Phys. Rev. Res.* **4**, 023244 (2022).
- [52] Z. Z. Liu *et al.*, *Charge-Density-Wave-Induced Bands Renormalization and Energy Gaps in a Kagome Superconductor*  $\text{RbV}_3\text{Sb}_5$ , *Phys. Rev. X* **11**, 041010 (2021).
- [53] Y. Hu *et al.*, *Topological Surface States and Flat Bands in the Kagome Superconductor*  $\text{CsV}_3\text{Sb}_5$ , *Sci. Bull.* **67**, 495 (2022).

- [54] H. Luo *et al.*, *Electronic Nature of Charge Density Wave and Electron-Phonon Coupling in Kagome Superconductor  $KV_3Sb_5$* , *Nat. Commun.* **13**, 273 (2022).
- [55] T. Kato *et al.*, *Three-Dimensional Energy Gap and Origin of Charge-Density Wave in Kagome Superconductor  $KV_3Sb_5$* , *Commun. Mater.* **3**, 30 (2022).
- [56] S. Cho *et al.*, *Emergence of New van Hove Singularities in the Charge Density Wave State of a Topological Kagome Metal  $RbV_3Sb_5$* , *Phys. Rev. Lett.* **127**, 236401 (2021).
- [57] M. Kang *et al.*, *Charge Order Landscape and Competition with Superconductivity in Kagome Metals*, *Nat. Mater.* **22**, 186 (2023)..
- [58] P. Wu *et al.*, *Unidirectional Electron-Phonon Coupling as a “Fingerprint” of the Nematic State in a Kagome Superconductor*, [arXiv:2302.05115](https://arxiv.org/abs/2302.05115).
- [59] L. Kautzsch *et al.*, *Incommensurate Charge-Stripe Correlations in the Kagome Superconductor  $CsV_3Sb_{5-x}Sn_x$* , [arXiv:2207.10608](https://arxiv.org/abs/2207.10608) (2022).
- [60] T. Kato, Y. Li, K. Nakayama, Z. Wang, S. Souma, M. Kitamura, K. Horiba, H. Kumigashira, T. Takahashi, and T. Sato, *Polarity-Dependent Charge Density Wave in the Kagome Superconductor  $CsV_3Sb_5$* , *Phys. Rev. B* **106**, L121112 (2022).
- [61] G. Kresse and J. Furthmüller, *Efficiency of Ab-Initio Total Energy Calculations for Metals and Semiconductors Using a Plane-Wave Basis Set*, *Comput. Mater. Sci.* **6**, 15 (1996).
- [62] G. Kresse and J. Furthmüller, *Efficient Iterative Schemes for Ab Initio Total-Energy Calculations Using a Plane-Wave Basis Set*, *Phys. Rev. B* **54**, 11169 (1996).
- [63] P. E. Blöchl, *Projector Augmented-Wave Method*, *Phys. Rev. B* **50**, 17953 (1994).
- [64] G. Kresse and D. Joubert, *From Ultrasoft Pseudopotentials to the Projector Augmented-Wave Method*, *Phys. Rev. B* **59**, 1758 (1999).
- [65] J. Perdew, K. Burke, and M. Ernzerhof, *Generalized Gradient Approximation Made Simple*, *Phys. Rev. Lett.* **77**, 3865 (1996).
- [66] A. A. Mostofi, J. R. Yates, G. Pizzi, Y.-S. Lee, I. Souza, D. Vanderbilt, and N. Marzari, *An Updated Version of Wannier90: A Tool for Obtaining Maximally-Localised Wannier Functions*, *Comput. Phys. Commun.* **185**, 2309 (2014).
- [67] W. Ku, T. Berlijn, and C.-C. Lee, *Unfolding First-Principles Band Structures*, *Phys. Rev. Lett.* **104**, 216401 (2010).